Causing the Effect: Driving the Unruh Response

Kevin Player

Software Engineering Institute
Carnegie Mellon University
kplayer@andrew.cmu.edu

August 30, 2025

> The Unruh effect tells us that what we call particles is really just a matter of perspective.

> <div align="right">Lee Smolin</div>

Abstract

We present a simple model that connects the Unruh effect to non-thermal entangled excitations produced from a bilocal driving source motivated by squeezing interactions in quantum optics. These paired excitations can be thought of as an inertial microstates in the accelerated thermal Unruh ensemble. The model reverses the usual story; rather than entanglement being a consequence of acceleration, we demonstrate how an acceleration response can itself be engineered. We then construct localized driving modes that avoid the asymptotic Doppler tails responsible for thermality. Using modular automorphisms, we track mode and observer localizations across nested Rindler wedges and construct compact wave-packet approximations with parabolic cylinder functions. These provide a smooth interpolation from global thermal Rindler modes to fully localized nonthermal excitations, and outline a program for understanding vacuum correlations as causally driven, nonthermal responses of the field.

1 Introduction

The Unruh effect [1] reveals that uniformly accelerated observers describe the Minkowski vacuum not as empty, but as a thermal bath of excitations. This apparent thermality reflects the deep entanglement structure of the vacuum: for inertial observers the Minkowski vacuum is pure and non-thermal, while for accelerated observers it appears as a mixed thermal state. Geometrically, uniform acceleration divides spacetime into left and right Rindler wedges, separated by an event horizon. The vacuum can be expressed as an entangled product of excitations across these wedges, so that tracing out one side yields a thermal description of the other. Local measurements in one wedge therefore have non-local implications for the other.

Recent work has explored the subtlety of this thermality, examining detector locality, causal structure, and the entanglement-information tradeoffs that underpin Unruh correlations. Anastopoulos and Savvidou [2] showed that while a single uniformly accelerated Unruh–DeWitt detector exhibits thermal fluctuations, correlations between two spatially

separated detectors with the same acceleration are nonthermal. This indicates that the Unruh effect is fundamentally local, with information encoded in correlations between distant observers. Foo, Onoe, and Zych [3] studied detectors in quantum superpositions of classical trajectories. Although each trajectory individually yields a thermal response, the superposed detector does not thermalize, demonstrating the importance of causal relations rather than acceleration alone.

Svidzinsky, Scully, and Unruh [4] analyzed causal chains of harmonic oscillators spanning both wedges. They found that the entanglement of the Minkowski vacuum transfers directly to the entanglement of oscillators interacting with the field, reinforcing the causal underpinning of Unruh correlations. Han, Olson, and Dowling [5] examined the role of measurement, showing that when an accelerating observer performs a projection-valued measurement (PVM), the field is driven out of its thermal character. For inertial observers the field is no longer vacuum, but contains real photons with nonzero energy–momentum, so the accelerated PVM acts as a process that injects energy and momentum through the accelerating agent itself.

In this work we develop a complementary viewpoint that inverts the usual narrative. Rather than acceleration generating entanglement, we construct a simple source-based model in which localized entangled emissions act as the causal origin of an acceleration response. These driven excitations provide concrete microstates consistent with the thermal Unruh ensemble, offering a minimal construction of how entanglement can manifest as accelerated dynamics. We also map out generalizations by considering backreaction, reversed emission and absorption, and related extensions.

In Section 2, we review the Unruh effect, including the relevant mode expansions and Bogoliubov transformations. In Section 3, we construct a bilocal source term, motivated by squeezed-state interactions in quantum optics, that injects correlated excitations into the field. Section 4 explores partial localization by considering sub-regions of the Rindler wedge connected through space-like translations and reflections, transformations that correspond to modular automorphisms in the associated operator algebras. We then use parabolic cylinder functions to construct a smooth interpolation between eternal Rindler modes and fully localized modes. Finally, in Section 5 we outline directions for future research, and in Section 6 we discuss connections to other research, and interpret the implications of our construction.

2   Preliminaries

We draw notation and standard results from Frodden and Valdés [6]. Let $\hbar = c = 1$. We work in 1+1 dimensional Minkowski spacetime with free, massless scalar fields, which capture the essential features of the Unruh effect without the overhead of higher dimensions or interactions. These simplifications preserve the relevant physics and clarify the constructions.

Consider the free scalar massless Lagrangian

$$\mathcal{L}_{free} = -\frac{1}{2}\eta^{\mu\nu}\partial_\mu\phi\partial_\nu\phi. \tag{1}$$

We consider positive frequency modes with dispersion relation $\omega_k = |k| > 0$ as solutions to the resulting Klein-Gordon equation

$$\Box\phi = -\frac{\partial^2\phi}{\partial t^2} + \frac{\partial^2\phi}{\partial x^2} = 0, \tag{2}$$

where $\Box = \eta^{\mu\nu}\partial_\mu\partial_\nu$. We expand ϕ in terms of ladder operators $a_k, a_k^\dagger$

$$\phi(x,t) = \int \mathrm{d}k\, a_k\varphi_k(x,t) + \text{h.c.} \tag{3}$$

where

$$\varphi_k(x,t) = \frac{1}{\sqrt{4\pi\omega_k}}e^{i(kx-\omega_k t)}. \tag{4}$$

are pure Minkowkski positive frequency waves normalized with respect to the Klein-Gordon inner product over a Cauchy surface Σ (usually $t = 0$)

$$\langle f,g\rangle_{KG} = i\int_\Sigma \mathrm{d}x(f^*\partial_t g - \partial_t f^* g). \tag{5}$$

2.1 Rindler Coordinates

To describe the physics from the point of view of a uniformly accelerating observer, we introduce Rindler coordinates [6, 7] covering a right wedge

$$W = \{(x,t) : x > |t|\} \tag{6}$$

with apex at the origin, pictured[1] in Figure 1; with coordinates

$$t = \frac{1}{a}e^{a\xi}\sinh(a\eta) \tag{7}$$

$$x = \frac{1}{a}e^{a\xi}\cosh(a\eta) \tag{8}$$

The constant acceleration parameter a is introduced explicitly to make the dependence on the Unruh temperature, $T = \frac{a}{2\pi}$, manifest in subsequent expressions. The coordinates (η, ξ) describe the proper time and spatial position of a uniformly accelerating observer, with constant ξ corresponding to hyperbolic trajectories in Minkowski spacetime.
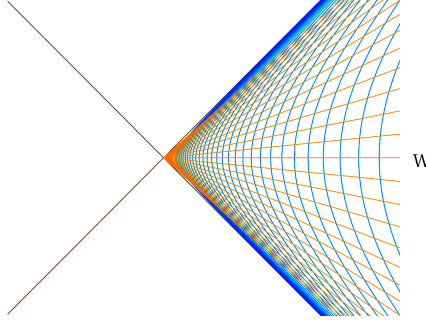

Figure 1: Rindler wedge W on the right, with Rindler coordinates.

The massless Klein-Gordon equation in Rindler coordinates is

$$\Box\phi = e^{-2a\xi}(-\partial_\eta^2 + \partial_\xi^2)\phi = 0 \tag{9}$$

The wave equation retains the same Minkowski structure up to the overall conformal factor $e^{-2a\xi}$. Since this factor does not affect the null structure of the equation, the mode solutions retain the same plane wave form but in the Rindler coordinates

$$r_k(\eta,\xi) = \frac{1}{\sqrt{4\pi\omega_k}}e^{-i(\omega_k\eta - k\xi)} + \text{h.c.} \tag{10}$$

for each wave number k and positive frequency $\omega_k = |k| > 0$. These Rindler modes are written in terms of η and ξ and are thus confined to the Rindler wedge W. Since Rindler coordinates only cover W (the right wedge), these modes are not defined globally in Minkowski space.

---

[1]All spacetime diagrams follow the convention of t increasing upward and x increasing to the right.

2.2 Unruh Modes

To review how a uniformly accelerated observer perceives the Minkowski vacuum as a thermal bath, we construct the Unruh modes[1], analytic continuations of Rindler modes that are positive-frequency solutions with respect to Minkowski time[2]. From now on let $\omega_k = k > 0$.

We define constants α_k and β_k, directly tied the the thermal description, which satisfy $\alpha_k^2 - \beta_k^2 = 1$

$$\alpha_k = \frac{e^{\frac{\pi\omega_k}{2a}}}{\sqrt{2\sinh\frac{\pi\omega_k}{a}}} = \sqrt{\frac{1}{1 - e^{-2\pi\omega_k/a}}} = \cosh\theta_k$$
$$\beta_k = \frac{e^{\frac{-\pi\omega_k}{2a}}}{\sqrt{2\sinh\frac{\pi\omega_k}{a}}} = \sqrt{\frac{1}{e^{2\pi\omega_k/a} - 1}} = \sinh\theta_k \quad \text{(thermal form)}$$

(11)

where θ_k is defined so that $\tanh\theta_k = \frac{\beta_k}{\alpha_k} = e^{-\pi\omega_k/a}$. These show up throughout in mode normalizations[3], inner products, and resulting Bogoliubov transforms. β_k also describes particle creation in terms of $|\beta_k|^2$ which has a thermal character, matching a Planck distribution at temperature $T = \frac{a}{2\pi}$.

Let $\widetilde{W}$ be the left Rindler wedge[4], $x < -|t|$ with Rindler modes $l_{\pm k}$. We analytically continue[5] the Rindler modes r_k, r_{-k}, l_k and l_{-k} into the (t, x) plane, these are the Unruh modes

$$\mu_{\pm k}^R = \frac{\alpha_k}{\sqrt{4\pi\omega_k}}(a(\mp t + x \pm i\epsilon))^{\pm\frac{i\omega_k}{a}} \qquad \mu_{\pm k|W}^R \to \alpha_k r_{\pm k}$$
$$\mu_{\pm k}^L = \frac{\alpha_k}{\sqrt{4\pi\omega_k}}(a(\mp t - x \pm i\epsilon))^{\pm\frac{i\omega_k}{a}} \qquad \mu_{\pm k|\widetilde{W}}^L \to \alpha_k l_{\pm k}$$

(12)

An $i\epsilon$ prescription selects the branch of the logarithm that renders the modes analytic and bounded on the half plane $\Im(t) < 0$. This makes the modes positive-frequency with respect to t. Another way of writing the Unruh modes is

$$\mu_{\pm k}^R = \alpha_k r_{\pm k} + \beta_k l_{\mp k}^*$$
$$\mu_{\pm k}^L = \alpha_k l_{\pm k} + \beta_k r_{\mp k}^*$$

(13)

where the right and left modes ($r_{\pm k}$ and $l_{\pm k}$) are understood to be zero outside of their respective wedges. See Figure 2 for an illustration of the various modes. The magnitude shown jumps across the branch cut and conjugates the phase. There are twice as many Unruh modes as Rindler modes, since each r_k appears with two analytic extensions, μ_k^R and μ_{-k}^{L*}, with a similar duplication for the left modes.

The Unruh modes form an alternative orthonormal basis of solutions to the Klein-Gordon equation, distinct from the plane waves $\varphi_{\pm k}$ see the original source Unruh[1]. The Unruh modes diagonalize (we will see in equation (17)) the Minkowski vacuum in terms of Rindler particle states and thus provide the natural framework for describing the Unruh effect and the thermal response perceived by uniformly accelerated observers.

2.3 Bogoliubov Transforms

We generalize the wedge W to a translated wedge W_c with apex $(0, c)$

$$W_c = \{(t, x) : x - c > |t|\}$$

(14)

---

[2] Positive frequency means that the modes contain no negative frequency Minkowski components.

[3] The normalizations come from computing the Klein Gordon inner product on Minkowski space and comparing it to inner products on W and $\widetilde{W}$.

[4] Coordinates on this wedge are $t = -\frac{1}{a}e^{a\delta}\sinh(a\gamma)$, $x = -\frac{1}{a}e^{a\delta}\cosh(a\gamma)$; and $l_{\pm k} = \frac{1}{\sqrt{4\pi\omega_k}}e^{i\omega_k(\gamma\pm\delta)}$.

[5] From the definitions and properties of sinh and cosh, it follows that $a(\pm t + x) = e^{a(\pm\eta+\xi)}$ and then $r_{\pm k} = e^{\pm\frac{i\omega_k}{a}\log a(\mp t + x \pm i\epsilon)}$ see [6] for details. Similar statements hold for the left wedge.

Figure 2: Spacetime diagrams of the $k > 0$ mode functions $\begin{bmatrix} \mu^L_{-k} & \varphi_k & \mu^R_k \\ \mu^L_k & \varphi_{-k} & \mu^R_{-k} \end{bmatrix}$ where μ and φ are Unruh modes and Minkowski mode respectively. Color encodes the phase; brightness indicates magnitude. The Unruh modes change magnitude and conjugate phase across the log branch according to the interpretation of $\log(-1 \pm i\epsilon)$. The left-moving modes (top) correspond to emission in Minkowski space; the right-moving modes (bottom) to absorption.

and a reflected (left) wedge $\widetilde{W}_c$ with apex $(0, c)$

$$\widetilde{W}_c = \{(t, x) : x - c < -|t|\}. \tag{15}$$

Let the superscripts (0), (c), $(\widetilde{c})$, and (M) represent the W_0, W_c, $\widetilde{W}_c$, and Minkowski frames of reference respectively. Let $(A \to B)$ represent an open set inclusion[6] $A \subseteq B$.

We directly compute $W_0 \to M$ Bogoliubov coefficients from equation (13) for a change of basis from $a_q^{(M)}$ to c_q^R and c_q^L

$$\phi = \int dq \; \mu_q^R c_q^R + \mu_q^L c_q^L + \text{h.c.} \tag{16}$$

We find a 4 by 4 block matrix with blocks of the form

$$\begin{bmatrix} a_k^{(0)} \\ a_{-k}^{\widetilde{(0)}\dagger} \end{bmatrix} = \begin{bmatrix} \alpha_k & \beta_k \\ \beta_k & \alpha_k \end{bmatrix} \begin{bmatrix} c_k^R \\ c_{-k}^{L\dagger} \end{bmatrix} \tag{17}$$

and three others, where the $a_{-k}^{\widetilde{(0)}\dagger}$ is a left wedge creation operator. We can summarize the transform in the right wedge W as

$$a_k^{(0)} = \alpha_k c_k^R + \beta_k c_{-k}^{L\dagger} \tag{18}$$

and three other similar relations for $a_{-k}^{(0)}$, $a_k^{(0)\dagger}$, and $a_{-k}^{(0)\dagger}$.

We now compute the general non-diagonal Bogoliubov transformations.

$$\begin{aligned} (c \to M): \quad a_k^{(c)} &= \int dq \; \alpha_{kq}^{(c \to M)} a_q^M + \beta_{kq}^{(c \to M)} a_q^{(M)\dagger} \\ (c \to 0): \quad a_k^{(c)} &= \int dq \; \alpha_{kq}^{(c \to 0)} a_q^{(0)} + \beta_{kq}^{(c \to 0)} a_q^{(0)\dagger} \\ (\widetilde{c} \to 0): \quad a_k^{(\widetilde{c})} &= \int dq \; \alpha_{kq}^{(\widetilde{c} \to 0)} a_q^{(0)} + \beta_{kq}^{(\widetilde{c} \to 0)} a_q^{(0)\dagger} \end{aligned} \tag{19}$$

---

[6]In the algebraic formulation of QFT, spacetime regions correspond to operator algebras. Here, we adopt a complementary (though formally contravariant) perspective, whereby shifts in the wedge induce Bogoliubov transformations between operator algebras.

The $(c \to M)$ coefficients involve a gamma function, arising from the KG inner product as an integral of an exponential phase from φ_k with a $(x - c)$ power from $r_k^{(c)}$ (the Mellin transform of e^{ikx} [8]):

$$
\begin{aligned}
\alpha_{kq}^{(c \to M)} &= \left\langle \varphi_q, r_k^{(c)} \right\rangle = \frac{1}{2\pi a} \sqrt{\frac{\omega_k}{\omega_q}} \left(\frac{a}{q} \right)^{\frac{i\omega_k}{a}} e^{\frac{\pi\omega_k}{2a}} \Gamma \left(\frac{i\omega_k}{a} \right) \\
\beta_{kq}^{(c \to M)} &= \left\langle \varphi_q^*, r_k^{(c)} \right\rangle = \frac{1}{2\pi a} \sqrt{\frac{\omega_k}{\omega_q}} \left(\frac{a}{q} \right)^{\frac{i\omega_k}{a}} e^{\frac{-\pi\omega_k}{2a}} \Gamma \left(\frac{i\omega_k}{a} \right)
\end{aligned}
\tag{20}
$$

Next we consider products of shifted powers to study $(c \to 0)$. We make use of a beta function for $(c \to 0)$ which occurs naturally in the KG dot product as an integral over a power of x and of $x - c$, from $r_k^{(0)}$ and $r_k^{(c)}$ respectively. We compute the Bogoliubov coefficients as

$$
\begin{aligned}
\alpha_{kq}^{(c \to 0)} &= \left\langle r_q^{(0)}, r_k^{(c)} \right\rangle = \frac{1}{2\pi a} \sqrt{\frac{\omega_k}{\omega_q}} (ac)^{\frac{i(\omega_k - \omega_q)}{a}} B \left(\frac{i\omega_k}{a}, \frac{-i(\omega_k - \omega_q)}{a} \right) \\
\beta_{kq}^{(c \to 0)} &= \left\langle r_q^{(0)*}, r_k^{(c)} \right\rangle = \frac{1}{2\pi a} \sqrt{\frac{\omega_k}{\omega_q}} (ac)^{\frac{i(\omega_k + \omega_q)}{a}} B \left(\frac{i\omega_k}{a}, \frac{-i(\omega_k + \omega_q)}{a} \right)
\end{aligned}
\tag{21}
$$

The reflected diamond wedge version also yields a beta function, but with a different form

$$
\begin{aligned}
\alpha_{kq}^{(\widetilde{c} \to 0)} &= \left\langle r_q^{(0)*}, r_k^{(\widetilde{c})} \right\rangle = \frac{1}{2\pi a} \frac{\sqrt{\omega_k \omega_q}}{\omega_q - \omega_k} (ac)^{\frac{i(\omega_k - \omega_q)}{a}} B \left(\frac{i\omega_k}{a}, -\frac{i\omega_q}{a} \right) \\
\beta_{kq}^{(\widetilde{c} \to 0)} &= \left\langle r_q^{(0)}, r_k^{(\widetilde{c})} \right\rangle = \frac{1}{2\pi a} \frac{\sqrt{\omega_k \omega_q}}{\omega_q + \omega_k} (ac)^{\frac{i(\omega_k + \omega_q)}{a}} B \left(\frac{i\omega_k}{a}, \frac{i\omega_q}{a} \right)
\end{aligned}
\tag{22}
$$

2.4 Modular Automorphisms

Comparing absolute magnitudes for M versus W_c shows independence from c.

$$
\begin{aligned}
\left| \alpha_{kq}^{(c_1 \to M)} \right|^2 &= \left| \alpha_{kq}^{(c_2 \to M)} \right|^2 \\
\left| \beta_{kq}^{(c_1 \to M)} \right|^2 &= \left| \beta_{kq}^{(c_2 \to M)} \right|^2
\end{aligned}
\tag{23}
$$

The c independence is expected in this case since Unruh radiation is translation invariant. We next turn to $(c \to 0)$ and also find c independence there

$$
\begin{aligned}
\left| \alpha_{kq}^{(c_1 \to 0)} \right| &= \left| \alpha_{kq}^{(c_2 \to 0)} \right| \\
\left| \beta_{kq}^{(c_1 \to 0)} \right| &= \left| \beta_{kq}^{(c_2 \to 0)} \right|
\end{aligned}
\tag{24}
$$

This invariance is more surprising than in the Minkowski case, as it implies that the expected number of excitations for a mode $r_k^{(c_2)}$ when expressed in the vacuum of W_{c_1},

$$
\int \mathrm{d}q \, |\beta_{kq}^{(c_2 \to c_1)}|^2
\tag{25}
$$

is invariant[7] under changes in both c_1 and c_2.

More explicitly using the form of the c term in equations (21) and (22) we have a transform matrix of Λ_c from W_0 to W_c

$$
\begin{bmatrix}
a_k^{(c)} \\
a_{-k}^{(c)} \\
\hline
a_k^{(c)\dagger} \\
a_{-k}^{(c)\dagger}
\end{bmatrix}
=
\underbrace{
\left[
\begin{array}{cc|cc}
A_c & 0 & B_c & 0 \\
0 & -A_c & 0 & -B_c \\
\hline
\overline{B}_c & 0 & \overline{A}_c & 0 \\
0 & -\overline{B}_c & 0 & -\overline{A}_c
\end{array}
\right]_{k,q}
}_{\Lambda_c}
\begin{bmatrix}
a_q^{(0)} \\
a_{-q}^{(0)} \\
\hline
a_q^{(0)\dagger} \\
a_{-q}^{(0)\dagger}
\end{bmatrix}
\tag{26}
$$

---

[7]Similar statements are true for reflected (diamond) wedges.

where $A_c = \alpha_{kq}^{(c \to 0)} = P_c A_1 P_c^{-1}$ and $B_c = \beta_{kq}^{(c \to 0)} = P_c B_1 P_c$ for a diagonal phase factor matrix

$$P_{c,rs} = \delta(r-s) c^{\frac{i\omega_r}{a}} = e^{\frac{i}{a} H \log c} \tag{27}$$

where H is the Rindler Hamiltonian associated with mode frequency ω_k. We can write Λ_c out compactly out as

$$\Lambda_c = Q_c \Lambda_1 Q_c^{-1} \tag{28}$$

where

$$Q_c = \begin{bmatrix} P_c, & 0 & 0 & 0 \\ 0 & P_c & 0 & 0 \\ 0 & 0 & P_c^{-1} & 0 \\ 0 & 0 & 0 & P_c^{-1} \end{bmatrix} \tag{29}$$

The composition of Bogoliubov transforms, $\Lambda_{nc} = \Lambda_c^n$, yields

$$\begin{aligned} Q_{nc} \Lambda_1 Q_{nc}^{-1} &= \Lambda_{nc} \\ &= (Q_c \Lambda_c Q_c)\left(Q_c^{-1} \Lambda_c Q_c\right) \cdots (Q_c \Lambda_c Q_c) \\ &= Q_c \Lambda_c^n Q_c^{-1} \end{aligned} \tag{30}$$

so that

$$\begin{aligned} \Lambda_c^n &= Q_c^{-1} Q_{nc} \Lambda_1 Q_{nc}^{-1} Q_c \\ &= Q_n \Lambda_1 Q_n^{-1} \end{aligned} \tag{31}$$

and more generally we have a one parameter unitary group under the modular parameter $x = \log c$, with generator $\frac{1}{a} H$ given by

$$\left\{ \Lambda_1^x = Q_x \Lambda_1 Q_x^{-1} : x \in \mathbb{R} \right\}. \tag{32}$$

Thus the Bogoliubov transformations between shifted wedges form a one-parameter group under translations of the apex, paralleling modular automorphism flow in algebraic QFT [9]. In contrast to traditional treatments emphasizing Lorentz boosts within a fixed wedge, this formulation reveals modular structure via spatially translated wedges.

Consider a sequence

$$W_{c_n} \subsetneq \cdots \subsetneq W_{c_i} \subsetneq \cdots \subsetneq W_{c_j} \subsetneq W_{c_2} \subsetneq W_{c_1} \tag{33}$$

Each inclusion $W_{c_i} \subsetneq W_{c_j}$ yields the same particle production, with fixed squared Bogoliubov magnitude $|\beta_{kq}|^2$, so the expected number of particles remains constant across all nested wedge pairs, independent of the specific values of c_i or c_j. We will briefly revisit this chain in Section 3.4. Also this is related to [4] where we also see casual chains which are of a similar nature.

3 Driving Sources

We now turn to a foundational question – *what, physically, accelerates the observer?* In standard Unruh-effect derivations, the acceleration is treated as given; here we supply a concrete mechanism in the form of a localized, entangled source, thereby shifting from a purely kinematic description to a dynamical, source-based picture

In Section 2 we introduced acceleration as a geometric feature, a coordinate choice, without reference to any underlying dynamical mechanism. Moreover, we have left unspecified both the observer's precise location within the Rindler wedge and the spatial origin of the detected excitations. These omissions reflect an effective coarse-graining over the details of the observer and their interaction with the field, a feature that contributes to the apparent thermality observed in the Unruh effect.

A natural physical interpretation is that a *driving source* must exist, both as the cause of the observer's acceleration, and as a localized source coupled to the quantum field. In

Figure 3: A Rindler mode's frequency is smeared out in Minkowski space, blue-shifted near the horizon, and red-shifted as x goes to positive infinity. We illustrate the process as a particle striking a mirror at the rear of a rocket, where its reflection emerges as a combination of emission and absorption processes in the Rindler frame.

this view, acceleration is not merely a kinematic artifact or coordinate reparameterization, but the result of active, localized interactions along the observer's worldline. These interactions are responsible for the observer's motion. This plays well with the notion that the observer is not in an isotropic background radiation, but is actually accelerated away from a thermal event horizon, the thrust being intimately correlated with the causal horizon.

Figure 3 illustrates the situation with a particle composed of Rindler modes on the right wedge. The modes r_k are left-moving, propagating toward the future horizon and associated with *emission*; the r_{-k} modes are right-moving, originating from the past horizon and are associated with *absorption*. These Rindler modes are constructed as superpositions of restricted Minkowski modes $\varphi_{q|_W}$ effectively smeared across a range of frequencies. This frequency mixing is evident in Figure 2, where the modes blueshift infinitely near the horizons and red-shift infinitely at spatial infinity, reflecting the geometry of the wedge.
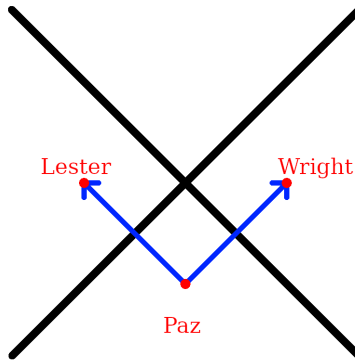
3.1   Construction

Figure 4: A thruster in the past, Paz(P), emits an entangled photon pair that accelerates Wright(R) (to the right) and Lester(L) (to the left).

We begin our construction of a driving source by following an Alice-and-Bob style naming convention, we use the names Wright (R), Lester (L), and Paz (P) to represent

observers at $(t, x) = (0, 1)$, $(0, -1)$, and $(-1, 0)$, respectively. These labels indicate Right, Left, and Past, serving as a mnemonic for their positions in spacetime. Paz serves as a common causal ancestor to Wright and Lester, and she emits an entangled pair of photons with momentum $\pm k$ and (Rindler) frequency $\omega = \omega_{\pm k}$ as part of a photon stream that, in our model, provides the correlated accelerations of Wright and Lester.

Because the emitted photons carry perfectly balanced momenta, our basic model exhibits no back reaction – this is a simplification – in more general models, single-particle sources would encode back reaction through their entanglement structure, see Section 3.2 and Figure 7.

The key novelty of our construction is the inversion of the usual logic. Instead of the usual localized detector model, an Unruh–DeWitt detector [1, 10] or a moving mirror [11], we place a source ('thruster') in the past. This exchanges the roles of detector and source, inverting effect and cause: where the standard picture begins with acceleration and finds entanglement, our construction begins with entanglement and produces acceleration.

Paz's emission makes the source of the acceleration manifest as particle injection, so that Wright will necessarily detect a particle with peaked right-moving momentum $-k$. Wright's detection is entangled with Lester's, and Lester will also observe a particle with left moving momentum k; measurement induced correlation.

Physically, Paz introduces a bilocal source

$$
\begin{aligned}
J(x, y) &= \lambda f_L(x) f_R(y) \\
\mathcal{L}_{sourced} &= \mathcal{L}_{free} + \frac{1}{2}\lambda \int f_L(x) f_R(y) \phi_+(x) \phi_+(y) + h.c. \\
&= \mathcal{L}_{free} + \frac{1}{2}\lambda \left(q_k^{L\dagger} q_{-k}^{R\dagger} + q_k^L q_{-k}^R \right)
\end{aligned}
\tag{34}
$$

with coupling constant λ, normalized mode profiles f_L and f_R supported on the left and right wedges respectively, creation operators $q_k^{L\dagger}$ and $q_{-k}^{R\dagger}$, and ϕ_+ as the positive frequency (annihilator) part of ϕ. The last part of equation (34) is the squeezing interaction for frequency ω, so that the bilocal source creates entangled particles in the Rindler basis within the wedges.

This source construction is a quadratic generalization of the usual linear source term [12] [13] and is motivated by quadrature squeezed light generation in quantum optics [14]; it is a coupling of a classical function J with the field as an interaction term smeared over x and y. In this model J squeezes the field creating correlations that manifest as entanglement at the level of a global quantum state. The product structure reflects this paired excitation.

We consider the case where f_L and f_R are absorptions, or made up of left moving and right moving Minkowkski modes respectively; the emission case is similar see Section 3.2. In this picture, the bilocal source is not just a mathematical device but the physical mechanism by which acceleration is generated: the entangled pair created by $J(x, y)$ supplies the correlated excitations that are experienced as thrust by the Rindler observers.

Smearing with ϕ_+ projects f_L and f_R onto their positive frequency parts which we call g_L and g_R respectively. In particular we can choose f_L and f_R to be Rindler modes l_k and r_{-k} in which case the projection is onto the corresponding Unruh modes μ_k and μ_{-k}, so that $q_k^{L\dagger}$ and $q_{-k}^{R\dagger}$ are the corresponding Unruh operators $c_k^{L\dagger}$ and $c_{-k}^{R\dagger}$[8].

We next consider the standard thermal vacuum description[9] of the Unruh effect

$$
|0\rangle_M = \prod_\omega \frac{1}{\cosh \theta_k} \sum_n \tanh^n \theta_k \, |n_\omega\rangle_L \, |n_\omega\rangle_R .
\tag{35}
$$

---

[8]See Section 2 equations (12), (13), and (16).

[9]The form of this vacuum equation can be proven by recursively applying the Bogoliubov relations from equation (18).

Table 1: Bilocal Source – Modes, Operators, and States

Type	Source	Projection	Operator	State (1st order)
General Left	f_L	g_L	$q_k^{L\dagger}$	$\lvert\psi\rangle_L$
General Right	f_R	g_R	$q_{-k}^{R\dagger}$	$\lvert\psi\rangle_R$
Rindler/Unruh Left	l_k	μ_k^L	$c_k^{L\dagger}$	$\lvert 1_\omega\rangle_L$
Rindler/Unruh Right	r_{-k}	μ_{-k}^R	$c_{-k}^{R\dagger}$	$\lvert 1_\omega\rangle_R$

A state that factorizes into correlated excitations in the left (L) and right (R) wedges. The Unruh modes associated with frequency ω are specific linear combination of these L and R Rindler modes, so that any source J coupling to it will, in general, drive correlated excitations across both wedges. For example, the state prepared by Paz with Rindler modes corresponds to a selective excitation at a fixed ω,

$$\lvert\Psi_\omega\rangle_M = \lvert 1_\omega\rangle_L \lvert 1_\omega\rangle_R + \mathrm{O}(\text{higher terms}), \tag{36}$$

a controlled realization of one term in the ensemble coming from the Rindler/Unruh modes. Our source projects the state onto the ω term through the act of observation, i.e. by a PVM projection in the standard quantum-measurement sense (see also [5]), so that Wright's guaranteed detection is modeled as the measurement-induced selection of a specific component of the thermal ensemble. The source $J(x,y)$ does not contradict the thermal interpretation, but rather describes a specific "microstate" consistent with the broader thermal ensemble.

An illustration of this setup is shown in Figure 5. From this perspective, the apparent thermality arises from intrinsic properties of the vacuum, an effective ignorance of the source's detailed structure and dynamics. In the sourced view, the Unruh effect is not a passive revelation of hidden particles in the vacuum, but a measurable consequence of *thrust*.
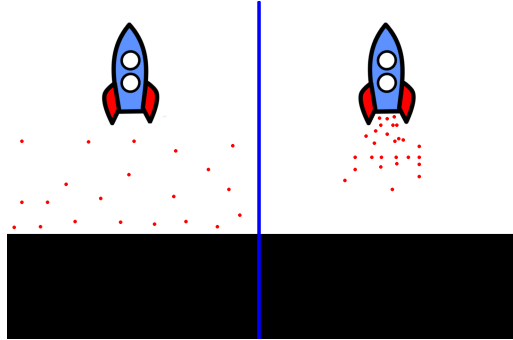

Figure 5: Conceptual illustration of thermal v.s. localized acceleration.

3.2   Physical Details

The construction of a right moving absorption function f_R for Wright presents some physical challenges.

- **Mode Projection**. We note that the f_L and f_R that match equation (36) are exactly the Rindler modes l_k and r_{-k} from Section 2. The source J is described in the Rindler wedges, and not immediately on the past wedge, so Paz will need to couple to Unruh modes – the analytically continued Rindler modes. We form f_R out of a linear combination of a left Unruh mode μ_k^{L*} and right Unruh mode μ_{-k}^R to get

r_{-k} supported on just the right wedge, see equation (13). The projection in equation (34) encodes this relation by projecting the Rindler modes onto Unruh modes or in more generality by projecting f_L and f_R onto positive frequency g_L and g_R.

- **Source over Finite Time**. We are integrating over the entire Minkowski space instead of over a short time period as normally desired for a source J. This challenge is met by noticing that the projected positive frequency modes g_L and g_R can be restricted and scaled on a small time interval $|t + 1| < \delta$ around Paz's time $t = -1$ to give the same result, see Figure 6 (right picture). This is because the integral over x is independent of t. This is manifestly evident by the fact that the mode is translation invariant over time and space, $g_R(t, x) = g_R(-1, x + t + 1)$, since it is a sum of right moving Minkowski modes. The coupling constant λ in equation (34), along with δ, can be chosen to match the vacuum equation (35) at $n_\omega = 1$.
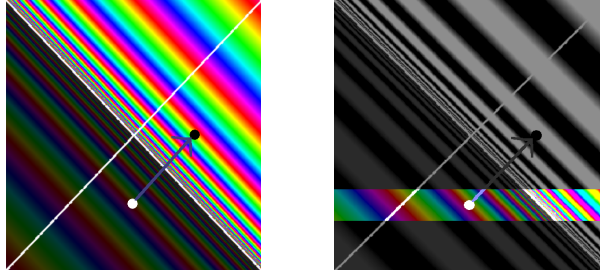

Figure 6: The points marked with black and white dots at (0,1) (Wright) and (-1,0) (Paz) respectively in the left picture lie on the same Unruh mode trajectory; although the mode is infinitely blue-shifted at the horizon, it settles down at Wright and Paz's locations. The right figure illustrates a finite time interval of width δ for the source J to be active. Note how each time slice is a translation of the time = -1 slice.

- **Blue Shifting near Horizon**. A third note is that the Unruh modes undergo an infinite blue shift at the horizon, but are more well behaved at Wright and Paz's locations[10]. We study the localization of functions on the right wedge in subsequent sections where we aim to attenuate or bound f_R away from the high-frequency, near-horizon behavior typical of thermal modes, making the physical realization of the source J more plausible as a wave packet.

- **Single Photon Models**. We mention that our running example represents just one of many possible mechanisms for exchanging energy and correlations between wedges; for example, in our symmetric two–mode setup, the momenta are balanced and the source does not experience recoil, so there is no back reaction. By contrast, if Paz emitted a single particle, as in Figure 7, the emitted mode would necessarily be entangled with Paz's internal state and/or recoil momentum, producing back reaction as field–source entanglement. Tracing out the source would leave Wright with a mixed state, and the apparent thermality would then arise from this entanglement with the thruster's degrees of freedom. Our choice of a balanced bilocal source thus isolates the thrust mechanism while postponing the additional complication of explicit source recoil for future research.

- **Emission** We could also study the emission case (we have been studying the absorption case); where f_L and f_R are made up of right moving and left moving Minkowski modes respectively. These would posit a common observer in the future. The moving mirror exemplifies aspects of both the "Emission" and "Single Photon Model"

---

[10] f_R is actually zero at Paz and in fact on the entire past wedge, but the projection g_R is an Unruh mode which is nonzero at Paz's location.
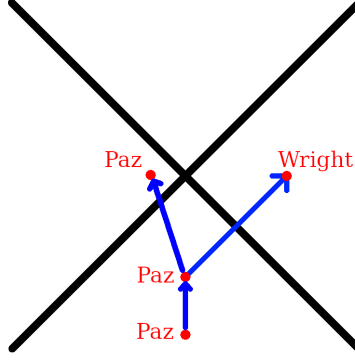
Figure 7: Paz emits a single photon and experiences a back reaction pushing her toward the left wedge. Through recoil she becomes entangled with the emitted particle, effectively taking on the role that Lester played in the symmetric construction.

cases. These cases involve additional complications beyond the scope of our short note and are a topic of future research.

For the remainder of this note, we focus on the function f_R in the right wedge without explicit reference to f_L, operating under the assumption that the localized driving source in the right wedge arises from a globally entangled paired source.

3.3 Heuristic Time-Reversed Narrative

The following discussion should be read as a heuristic narrative rather than a literal dynamical account; it illustrates how the time orientation of Rindler wedges lends itself to a "back in time" story that mirrors the entanglement structure. Wright's proper time (Right Rindler time) is by convention set up to be in the same direction[11] as Minkowski time. By contrast, Lester's proper time (Left Rindler time) in the left wedge is flowing in a direction[12] reverse to Minkowski time. This can be heuristically described as:

1. Lester *emits* a particle traveling back in time.

2. Paz receives this particle and reflects it forward in time to Wright.

3. Wright then absorbs the particle.

The presence of virtual particle-antiparticle pairs in massive scalar fields further enriches this picture, where antiparticles are understood as particles moving "back in time", though this extension lies beyond the scope of this present note.

We can interchange these emission and absorption stories, see "Emission" in Section 3.2, Wright emits and Lester absorbs, but we would need to involve an observer in the future say at $(t, x) = (1, 0)$ for that.

3.4 Sub-Wedge Causal Chain

The sub-wedge sequence mentioned in equation (33) has an interesting interpretation. The vacuums are entangled from each wedge to the next sub-wedge, and each sub-wedge has vacuum particle expectations of the same character. In our construction, this is understood as a causal chain from Paz to Wright. Each sub-wedge inherits a source J and f_R from the previous. This is also related to [4] where we also study causal chains from a common source.

---

[11]since $\partial_\eta = a(t\partial_x + x\partial_t)$
[12]since $\partial_\gamma = -a(t\partial_x + x\partial_t)$

4 Localization

Up to now, our modes have been perfectly sharp in Rindler frequency. We now construct various localization techniques. From this point we use "Rindler" and "Unruh" modes interchangeably when restricted to a single wedge, as our focus is the localized support.

4.1 Localization via Translated Wedge Inclusion

Consider the two nested Rindler wedges $W_c \subsetneq W_0$ shown in Figure 8. Let r_q denote a Rindler mode associated with W_0, analytically continued to the entire Minkowski space. The gray-scale region indicates the full support of r_q, while the rainbow-colored segment shows its restriction to the sub-wedge W_c.
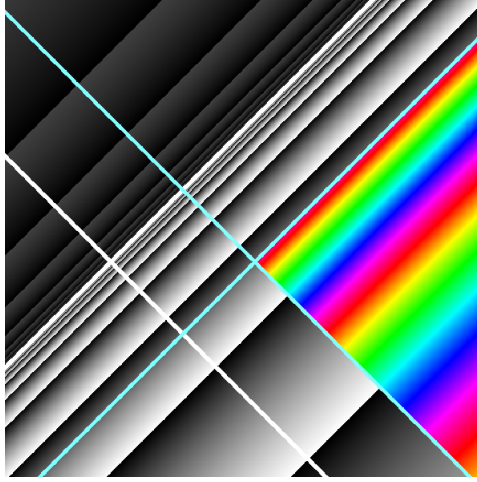

Figure 8: A Wedge W_c (cyan) inside of the wedge W_0 (white). Rindler mode r_q of W_0 (gray-scale) restricted to W_c (rainbow).

By considering the restriction of r_q to W_c, we have partially localized the observer and the mode. The restriction cuts off the high-frequency content of r_q near the future horizon[13] of W_0. The resulting mode still spans the full spatial extent of W_c, but avoids the highly oscillatory behavior near the horizons of W_0. The localization is not complete however, the observer can still be anywhere within the wedge W_c, and the corresponding modes r_k still exhibit thermal characteristics because of low-frequency oscillations extending as $x \to \infty$.

To further study the situation we first review the Minkowski/Rindler situation by fixing q and considering the modulus squared inner product $\left|\left\langle \varphi_q, r_k^{(c)} \right\rangle\right|^2$ also known as the Bogoliubov $\left|\alpha_{kq}^{(0\to M)}\right|^2$, from equation (20) . Using $|\Gamma(ib)|^2 = \frac{\pi}{b \sinh \pi b}$ we obtain the thermal response coming from the α_k term in

$$\left|\left\langle \varphi_q, r_k^{(c)} \right\rangle\right|^2 = \frac{1}{2\pi\omega_q} \left(\frac{1}{1 - e^{-\frac{2\pi\omega_k}{a}}} \right) \tag{37}$$

We graph a scaled version of this response as the red curve in Figure 9.

In contrast we next consider the modulus squared inner product $\left|\left\langle r_q^{(0)}, r_k^{(c)} \right\rangle\right|^2$, also known as the Bogoliubov $\left|\alpha_{kq}^{(c\to 0)}\right|^2$, from equation (21). We obtain

$$\left|\left\langle r_q^{(0)}, r_k^{(c)} \right\rangle\right|^2 = \frac{\sinh \frac{\pi\omega_q}{a}}{4\pi a(\omega_q - \omega_k) \sinh \pi \frac{\omega_q - \omega_k}{a} \sinh \frac{\pi\omega_k}{a}} \tag{38}$$

---

[13]Similarly, r_{-q} experiences suppression near the past horizon.

as a function of ω_k. The function exhibits a second-order pole at $\omega_k = \omega_q$, resulting in a sharply peaked feature, see the "complete Beta" green curve in Figure 9. Although the sinh terms encode aspects of the familiar thermal distribution, especially broadening near $\omega_k = 0$, the existence of the peak itself at $\omega_k = \omega_q$ originates from the geometric restriction, absent in the Minkowski/Rindler overlap.
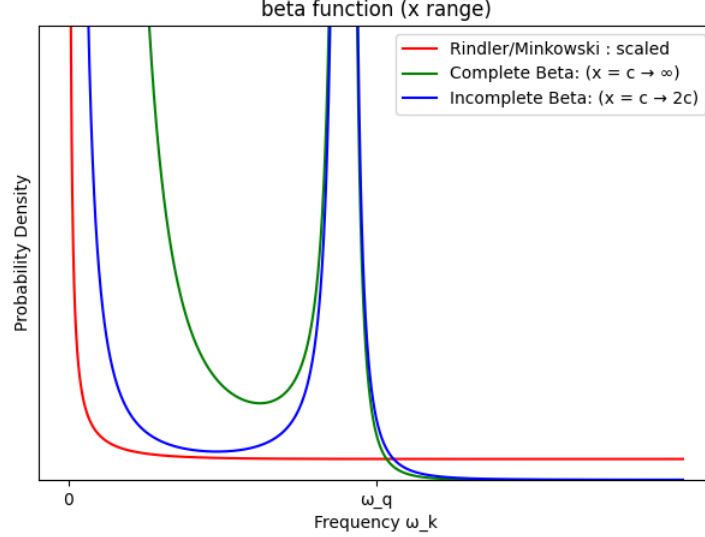

Figure 9: The Rindler modes r_k of W_c show a peaked spectral overlap with r_q at $\omega_k = \omega_q$ (green). The incomplete beta function (blue) strengthens the spectral peak and suppresses the peak at zero. Compare with purely thermal Minkowski/Rindler (red) curve.

4.2 Diamond Localization via Reflected Wedge Intersection

Further localization results from intersecting W_c with a reflected wedge $\widetilde{W}_{2c}$. This defines a more tightly localized diamond-shaped region, shown in Figure 10. The mode r_q is now restricted to the intersection $W_c \cap \widetilde{W}_{2c}$, which eliminates much of the infrared behavior previously associated with the unrestricted wedge.

The Klein Gordon inner product at $t = 0$ now takes the form of an incomplete version of the beta function from equation (21), corresponding to an integral[14] evaluated from c to $2c$ rather than extending to infinity. This inner product does not however correspond to a mode expansion of the field, since we restrict the support to the diamond. So the construction does not define a complete orthonormal set, and cannot be used to build a full basis of field modes on the entire wedge.

Accordingly we instead interpret r_q as part of a global mode expansion, we regard it as a compactly supported, non-invariant test function, i.e., a driving source localized to the diamond region, consistent with the source framework introduced in Section 3. We turn on r_q exactly for a fixed period of $x - t$ (or $x + t$ for r_{-q}). The resulting spectral response in the diamond, computed from this truncated integral, is shown[15] as the blue curve in Figure 9. The plot reveals that the main spectral peak at $\omega_k = \omega_q$ persists, while the thermal contribution near $\omega = 0$ is significantly attenuated.

---

[14]We could also use the other form of the beta function in equation (22) to compute the same inner product.

[15]The complete (green) beta function curve is actually independent of the choice of translation c, it is the same curve for any sub-wedge space-like inclusion (see modular automorphism Section 2.4). In contrast, the incomplete beta function curve (blue) does depend on the endpoint ($2c$ is shown).
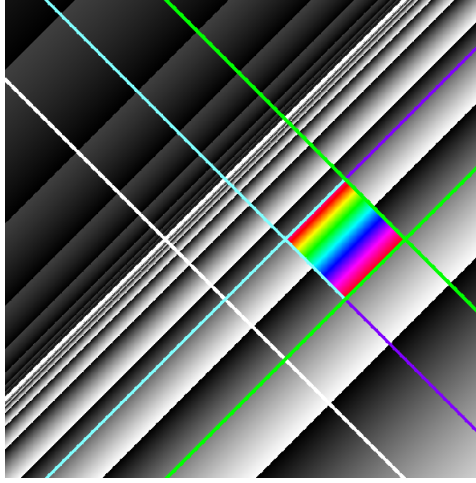
Figure 10: The same situation as in Figure 8 but we further intersect with a reflected (left) wedge $\widetilde{W}_{2c}$ (green). Rindler mode r_q of W_0 (gray-scale) restricted to $W_c \cap \widetilde{W}_{2c}$ (rainbow).

4.3 Thermal to Localized Interpolation

To further probe how global thermal structure transitions into a localized excitation, we consider the behavior of Rindler-to-Minkowski Bogoliubov coefficients when weighted by a Gaussian envelope. This allows us to interpolate between de-localized (thermal) and localized (spectrally peaked) behavior. We use parabolic cylinder functions [15, 16] which are the analytic continuation of

$$D_\nu(-z) = \frac{e^{-\frac{1}{4}z^2}}{\Gamma(-\nu)} \int_0^\infty ds\ e^{zs} s^{-\nu-1} e^{-\frac{1}{2}s^2}, \Re\nu < 0, \tag{39}$$

where we use $-z$ instead of the usual z so that future equations become simpler.

Without loss of generality, let $N_{\mu,\sigma} = e^{-\frac{1}{2}\frac{(x-t-\mu)^2}{\sigma^2}}$ be a (left-moving) Gaussian kernel with fixed μ. We will multiply φ_q^* by $N_{\mu,\sigma}$, but we could just as easily multiply r_k by $N_{\mu,\sigma}$ for the same effect. Here the resulting Minkowski modes are treated as driving sources rather than elements of an orthonormal mode expansion. Since we are not working within an orthonormal mode expansion, the normalization of $N_{\mu,\sigma}$ is left implicit. Since this setup is non-standard, we give the explicit calculations. We will examine the $N_{\mu,\sigma}$ modification of $\beta_{kq}^{(c\to M)}$ in equation (20)

$$
\begin{aligned}
\langle \varphi_q^* N_{\mu,\sigma}, r_k \rangle &= \frac{1}{4\pi\sqrt{\omega_q \omega_k}} 2i \int_{\Sigma_W} e^{-i(\omega_q t - qx)} e^{-\frac{1}{2}\frac{(x-t-\mu)^2}{\sigma^2}} \partial_t (a(x-t))^{\frac{i\omega_k}{a}} \\
&= \frac{1}{2\pi}\sqrt{\frac{\omega_k}{\omega_q}} a^{\frac{i\omega_k}{a}-1} \int_0^\infty dx\ e^{-\frac{1}{2}\frac{(x-\mu)^2}{\sigma^2}+iqx} x^{\frac{i\omega_k}{a}-1} \\
&= \frac{1}{2\pi}\sqrt{\frac{\omega_k}{\omega_q}} a^{\frac{i\omega_k}{a}-1} \int_0^\infty dx\ e^{\left(-\frac{1}{2\sigma^2}\right)x^2 + \left(\frac{\mu}{\sigma^2}+iq\right)x + \left(-\frac{\mu^2}{2\sigma^2}\right)} x^{\frac{i\omega_k}{a}-1} \\
&= \frac{1}{2\pi a}\sqrt{\frac{\omega_k}{\omega_q}} e^{-\frac{\mu^2}{2\sigma^2}} \sigma^{\frac{i\omega_k}{a}} a^{\frac{i\omega_k}{a}} \int_0^\infty ds\ e^{\left(\frac{\mu}{\sigma}+iq\sigma\right)s} s^{\frac{i\omega_k}{a}-1} e^{-\frac{1}{2}s^2} \\
&= \frac{1}{2\pi a}\sqrt{\frac{\omega_k}{\omega_q}} e^{-\frac{\mu^2}{2\sigma^2}} (\sigma a)^{\frac{i\omega_k}{a}} e^{\frac{1}{4}(iq\sigma+\frac{\mu}{\sigma})^2} \Gamma\left(\frac{i\omega_k}{a}\right) D_{-\frac{i\omega_k}{a}}\left(-iq\sigma - \frac{\mu}{\sigma}\right) \\
&= \frac{1}{2\pi a}\sqrt{\frac{\omega_k}{\omega_q}} e^{-\frac{\mu^2}{2\sigma^2}} (\sigma a)^{\frac{i\omega_k}{a}} e^{\frac{1}{4}z^2} \Gamma(-\nu) D_\nu(-z)
\end{aligned}
\tag{40}
$$

where Σ_W is the Cauchy surface $\eta = 0$ on the Rindler wedge W, $x = \sigma s$, $z = iq\sigma + \frac{\mu}{\sigma}$, and $\nu = -\frac{i\omega_k}{a}$. And then

$$\left|\left\langle \varphi_q^* N_{\mu,\sigma}, r_k \right\rangle\right|^2 = \frac{1}{2\pi a\omega_q} \frac{\omega_k}{2\pi a} e^{-\frac{\mu^2}{\sigma^2}} \left|e^{\frac{1}{2}z^2}\right| |\Gamma(-\nu)|^2 |D_\nu(-z)|^2 \tag{41}$$
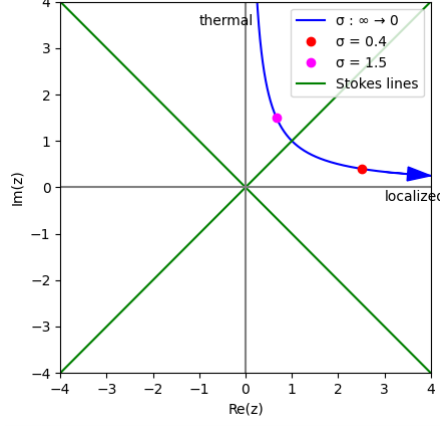
From [16] we have

Figure 11: Trajectory of $z = iq\sigma + \frac{\mu}{\sigma}$ as σ interpolates between thermal and localized regimes. For σ starting at ∞, the trajectory starts at the positive infinite imaginary axis, aligning with the dominant thermal component of the excitation. As $\sigma \to 0$, the system crosses a Stokes line and transitions into a sharply localized, source-driven configuration, where thermal character disappears. See also corresponding Figure 12.

$$D_\nu(-z) = e^{-i\pi\nu} z^\nu e^{-\frac{1}{4}z^2}\{1 + O(|z|^{-2})\} + \frac{(2\pi)^{\frac{1}{2}}}{\Gamma(-\nu)} z^{-\nu-1} e^{\frac{1}{4}z^2}\{1 + O(|z|^{-2})\} \tag{42}$$

when $-\frac{1}{4}\pi + \epsilon \le \arg z \le \frac{3}{4}\pi - \epsilon$.

The two asymptotic regimes correspond to physically distinct interpretations: The second $e^{\frac{1}{4}z^2}$ term dominates for $z \to \infty$ as $\sigma \to 0$ and the first $e^{-\frac{1}{4}z^2}$ term dominates for $z \to i\infty$ as $\sigma \to \infty$. This is a Stokes phenomenon[16] which flips over as we cross the Stokes line at $\arg z = \frac{\pi}{4}$. The situation is pictured in Figure 11.

We next combine equations (41) and (42). First for the thermal part that comes from the $e^{-\frac{1}{4}z^2}$ term where $\sigma \to \infty$ we have

$$\begin{aligned}
2\pi a\omega_q \left|\left\langle \varphi_q^* N, r_k \right\rangle\right|^2 &= \frac{\omega_k}{2\pi a} e^{-\frac{\mu^2}{\sigma^2}} \left|e^{-i\pi\nu} z^\nu \Gamma\left(\frac{i\omega_k}{a}\right)\right|^2 \\
&= \frac{\omega_k}{2\pi a} e^{-\frac{\mu^2}{\sigma^2}} e^{\frac{-2\pi\omega_k}{a}} \left|e^{\frac{-2i\omega_k}{a}\log\left(\frac{\mu}{\sigma}+iq\sigma\right)}\right|^2 \frac{\pi}{\frac{\omega_k}{a}\sinh\frac{\pi\omega_k}{a}} \\
&\to e^{\frac{-2\pi\omega_k}{a}} \left|e^{\frac{-2i\omega_k}{a}\log i}\right|^2 \frac{1}{2\sinh\frac{\pi\omega_k}{a}} \\
&= e^{\frac{-2\pi\omega_k}{a}} e^{\frac{\pi\omega_k}{a}} \frac{1}{\left(e^{\frac{\pi\omega_k}{a}} - e^{\frac{-\pi\omega_k}{a}}\right)} \\
&= \frac{1}{e^{\frac{2\pi\omega_k}{a}} - 1}
\end{aligned} \tag{43}$$

---

[16]See [17] for a similar situation where the Stokes phenomenon is applied to particle production in simple expanding backgrounds, preheating after R^2 inflation, and a transition model with smoothly changing mass.
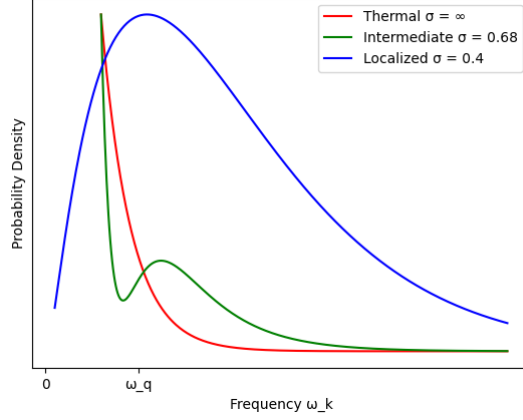
Figure 12: $\left|\left\langle\varphi_q^* N, r_k\right\rangle\right|^2$ for various values of σ (probability density is scaled for comparison). $\omega_q = 1$, $q = 1$, $a = 1$, $\mu = 1$. See also corresponding Figure 11.

which we expect by construction. For the localized part that comes from the $e^{\frac{1}{4}z^2}$ term where $\sigma \to 0$ we have

$$
\begin{aligned}
2\pi a \omega_q \left|\left\langle\varphi_q^* N, r_k\right\rangle\right|^2 &= \frac{\omega_k}{a} e^{-\frac{\mu^2}{\sigma^2}} \left|e^{z^2} z^{2(-\nu-1)}\right| \\
&= \frac{\omega_k}{a} e^{-\frac{\mu^2}{\sigma^2}} \left|e^{\left(iq\sigma+\frac{\mu}{\sigma}\right)^2} e^{2\left(\frac{i\omega_k}{a}-1\right)\log\left(iq\sigma+\frac{\mu}{\sigma}\right)}\right| \\
&\to \frac{\omega_k}{a} e^{\frac{-2\epsilon\omega_k}{a}} f(\sigma,\mu)
\end{aligned}
\tag{44}
$$

where the thermal pole at zero has disappeared. While the precise asymptotic form is not critical, we can control the ultraviolet behavior by taking z to $(1+i\epsilon)\infty$ which remains within in the localized Stokes region. This introduces a regulating factor of the form $e^{-2\epsilon\omega_k/a}$, which suppresses high-frequency contributions.

We restrict attention to small but finite σ, and $\sigma \to 0$ corresponds to a vanishing source rather than a delta function. We focus on the small-but-nonzero σ regime where the thermal character is already suppressed. See Figure 12 for representative plots across varying values of σ.

5   Future Research

Several directions naturally extend the present work:

- **Moving Mirrors**.

  A moving mirror can be viewed as both a detector and a "thruster" (Section 3); in this work the thruster and detector roles were treated separately. Extending the framework to include moving mirror timeline localizations remains open.

- **Mode Pairing**. The construction of f_L in Section 3 was not pursued in Section 4. A systematic analysis of the f_L–f_R pairing could clarify correlation structures more generally.

- **Alternative Driving Source Models**. Beyond entangled emission, models with single-photon sources or time-reversed scenarios (Section 3.2) may provide finer control over entanglement structure.

- **Massive Fields**. Extending the analysis to massive scalar fields would enable the study of localized virtual particle–antiparticle pair production, complementing the massless case.

17

- **Curved Spacetimes**. While our analysis is grounded in flat spacetime, the equivalence principle offers a natural pathway to curved geometries. In particular, applications to Hawking radiation could be explored by modeling localized excitations near black hole horizons. Figure 13 illustrates this direction, highlighting a shift from thermal emission to localized, physically sourced excitations in the near-horizon region.
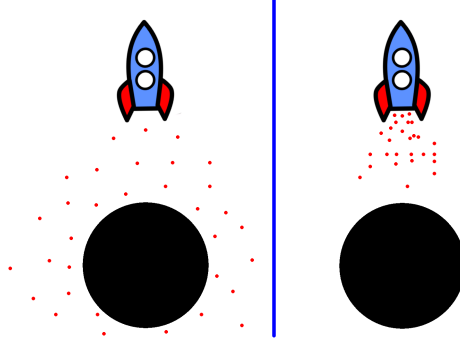

Figure 13: Conceptual illustration contrasting global Hawking radiation (left) with a localized, source-driven excitation near a black hole (right). Compare with Figure 5.

6 Conclusion

We have presented a framework in which individual microstates of the thermal Unruh ensemble are realized as physically localized, source-driven excitations, making the role of acceleration explicit rather than purely kinematic. We consider localization via wedge-restricted Rindler/Unruh modes and then construct compact wave-packets via parabolic cylinder functions. This provides a smooth interpolation between global Rindler modes and localized spectral structures.

Our construction complements the standard detector-based interpretation by showing how apparent thermality can coexist with microstate-level descriptions.

The framework suggests several directions for further investigation, including systematic mode pairing, moving mirror analogues, generalizations to massive fields, and potential extensions to curved spacetimes, with applications to near-horizon excitations in black hole physics.

7 Acknowledgments

References

[1] W. G. Unruh, "Notes on black-hole evaporation," *Physical Review D*, vol. 14, no. 4, p. 870, 1976.

[2] C. Anastopoulos and N. Savvidou, "Coherences of accelerated detectors and the local character of the unruh effect," *Journal of mathematical physics*, vol. 53, no. 1, 2012.

[3] J. Foo, S. Onoe, and M. Zych, "Unruh-dewitt detectors in quantum superpositions of trajectories," *Physical Review D*, vol. 102, no. 8, p. 085013, 2020.

[4] A. Svidzinsky, M. Scully, and W. Unruh, "Minkowski vacuum entanglement and accelerated oscillator chains," *Physical Review D*, 2024.

[5] M. Han, S. J. Olson, and J. P. Dowling, "Generating entangled photons from the vacuum by accelerated measurements: Quantum-information theory and the unruh-davies effect," *Physical Review A—Atomic, Molecular, and Optical Physics*, vol. 78, no. 2, p. 022302, 2008.

[6] E. Frodden and N. Valdes, "Unruh effect: Introductory notes to quantum effects for accelerated observers," *International Journal of Modern Physics A*, vol. 33, no. 27, p. 1830026, 2018.

[7] W. Rindler, "Kruskal space and the uniformly accelerated frame," *Am. J. Phys*, vol. 34, no. 12, pp. 1174–1178, 1966.

[8] R. Bracewell and P. B. Kahn, "The fourier transform and its applications," *American Journal of Physics*, vol. 34, no. 8, pp. 712–712, 1966.

[9] H. J. Borchers, "On revolutionizing quantum field theory with tomita's modular theory," *Journal of mathematical Physics*, vol. 41, no. 6, pp. 3604–3673, 2000.

[10] A. Einstein, *General Relativity: An Einstein Centenary Survey*. Cambridge University Press, 1979.

[11] S. A. Fulling and P. C. Davies, "Radiation from a moving mirror in two dimensional space-time: conformal anomaly," *Proceedings of the Royal Society of London. A. Mathematical and Physical Sciences*, vol. 348, no. 1654, pp. 393–414, 1976.

[12] J. Schwinger, "Particles and sources," *Physical Review*, vol. 152, p. 1219â€"1226, Dec. 1966.

[13] L. H. Ryder, *Quantum field theory*. Cambridge university press, 1996.

[14] C. C. Gerry and P. L. Knight, *Introductory quantum optics*. Cambridge university press, 2023.

[15] M. Abramowitz and I. A. Stegun, eds., *Handbook of Mathematical Functions with Formulas, Graphs, and Mathematical Tables*, vol. 55 of *Applied Mathematics Series*. Washington, D.C.: U.S. Government Printing Office, 1964. Reprinted 1983. See Chapter 19.

[16] F. W. J. Olver, "Uniform asymptotic expansions for weber parabolic cylinder functions of large orders," *Journal of Research of the National Bureau of Standards. Section B, Mathematical Sciences*, vol. 63B, pp. 131–169, 1959.

[17] S. Hashiba and Y. Yamada, "Stokes phenomenon and gravitational particle production—how to evaluate it in practice," *Journal of Cosmology and Astroparticle Physics*, vol. 2021, no. 05, p. 022, 2021.

[18] N. Beisert, "Quantum field theory i," *ETH Zurich, HS12*, 2012.